Applied Catalysis B: Environmental 184 (2016) 347–354

Contents lists available at ScienceDirect

Applied Catalysis B: Environmental

journal homepage: www.elsevier.com/locate/apcatb

Morphology engineering of V_2O_5/TiO_2 nanocomposites with enhanced visible light-driven photofunctions for arsenic removal

Liyan Xie[a], Ping Liu[b,**], Zuyang Zheng[b], Sunxian Weng[b], Jianhui Huang[a,*]

[a] College of Environmental and Biological Engineering, Putian University, Putian 351100, PR China
[b] Research Institute of Photocatalysis, State Key Laboratory of Photocatalysis on Energy and Environment, College of Chemistry and Chemical Engineering, Fuzhou University, Fuzhou 350002, PR China

ARTICLE INFO

Article history:
Received 14 August 2015
Received in revised form 4 November 2015
Accepted 14 November 2015
Available online 26 November 2015

Keywords:
V_2O_5/TiO_2 nanocomposites
Arsenic removal
Photocatalytic oxidation
Morphology control
Superoxide radical
Photo-generated holes

ABSTRACT

Morphological synthesis of V_2O_5/TiO_2 nanocomposites with unique core–shell spherical nanostructures and solid sphere nanostructures were achieved by solvothermal method and hydrothermal method, respectively. Owing to their intrinsic semiconductive properties and different nanostructures, both of these two nanocomposites were employed as solar energy transducers to photo-oxidation of arsenic (III) in aqueous solution, with the purpose to better understanding the morphological effect in photocatalysis. It clearly demonstrated that V_2O_5/TiO_2 with core–shell spheres morphology exhibited an excellent photocatalytic activity in the oxidation of arsenite (about 92%), remarkably superior to the one with solid sphere nanostructure, because of its larger specific surface area, enhanced visible harvest ability and improved charge separation efficiency. Furthermore, we discovered that superoxide radicals and photo-generated holes are the active species responsible for the oxidation of As(III) in the V_2O_5/TiO_2 photocatalytic system.

1. Introduction

In recent years, arsenic pollution in aquatic environment is becoming increasingly serious and threatening millions of people and other living beings around the world [1,2]. Due to its properties such as carcinogenicity and mutagenicity, the arsenic (As) leaching from minerals or contaminated soils shows highly toxic effect on living beings [3]. Long-term exposure to arsenic-containing water can lead to various kinds of cancers. Therefore, how to treat arsenic-containing wastewater economically and efficiently has been arousing intense interest from both academic and industrial societies.

It is well known that the toxic character of arsenic depends on its binding form. Inorganically bound species are more toxic than natural organically bound arsenic [4]. While the dominating forms of inorganic arsenic species in nature water are usually in the oxidation states of As(III) and As(V). Comparing to As(V), the As(III) is much more mobile in nature water and is more toxic than As(V) [5,6]. Besides when pH value is less than 9, the As(III) exists mainly in nonionic form H_3AsO_3, which is hard to remove by simple coagulation/precipitation or adsorption [7,8]. Therefore, the pre-oxidation treatment of As(III) to As(V) is quite necessary for the perspective of reducing the toxicity of arsenic and facilitating the immobilization and removal of arsenic [9].

It has been reported that the oxidation of As(III) can be achieved by various oxidants such as oxygen, ozone, hydrogen peroxide, manganese oxides, chlorine, ferrous, etc [10–12]. Among various treatment processes which have been reported to transform As(III) to As(V), the photocatalytic oxidation has been proven to be an effective and environmentally acceptable technique [4,13–15].

By far, TiO_2 as the most renowned semiconductor material has been exploited to the oxidation of arsenite in aqueous suspensions [11,16–18]. However, due to its band gap (~3.2 eV), TiO_2 can only be activated by UV light ($\lambda < 387$ nm), which can not make full use of the incoming solar energy. So, it is significant to expand the absorption band of TiO_2-based photocatalysts to visible light range. One of the main approaches to develop visible light response photocatalysts is coupling titania with another semiconductor which can extend optical absorption towards the visible part of the spectrum, for instance, Bi_2O_3/TiO_2 [19], Bi_2S_3/TiO_2 [20], In_2O_3/TiO_2 [21], WO_3/TiO_2 [22], $InVO_4/TiO_2$ [23], etc. As one of the most important metal oxides catalysts with a narrow band gap, V_2O_5 has been mixed with TiO_2 by various methods and exhibited visible-light-induced catalytic activity [24,25]. As all we known that both

* Corresponding author. Fax: +86 594 2676022.
** Corresponding author. Fax: +86 591 83779239.
E-mail addresses: liuping@fzu.edu.cn (P. Liu), owenhuang95@163.com (J. Huang).

http://dx.doi.org/10.1016/j.apcatb.2015.11.014
0926-3373/

the composition and the morphostructure play important roles in determining photocatalytic performance. Even the same photocatalysts with different microstructures like mesoporous, nanowires, nanosheets, hollow nanocrystals or core–shell microspheres will exhibit different catalytic activity [26–28]. Therefore, V_2O_5/TiO_2 composites with different morphologies may exhibit distinct photocatalytic performance.

In this paper, the V_2O_5/TiO_2 composites with different morphologies were synthesized by hydrothermal method and solvothermal method respectively, and the two V_2O_5/TiO_2 samples were used for the photocatalytic removal of arsenic from aqueous solution. Under visible light irradiation, two V_2O_5/TiO_2 samples exhibit distinct photocatalytic activity from each other in the oxidation of arsenite to arsenate. The role of active species during the photocatalytic oxidation process is also investigated in detail. It is expected that the core–shell structure V_2O_5/TiO_2 can act as a promising visible-light photocatalyst in the oxidation and removal of As(III).

2. Experimental section

2.1. Preparation

2.1.1. Materials

Absolute ethyl alcohol (99%), absolute ether (99%; Sinopharm Group), glycerol, ammonium metavanadate (A.R.), titanium oxysulfate (15 wt.% solution in dilute sulfuric acid; Adrich) were purchased from Sinopharm Chemical Reagent Co.. Deionized water was used throughout this study. 5,5-Dimethyl-1-pyrroline *N*-oxide (DMPO) was used as radicals spin trap and obtained from Alfa Aesar. Other commercial chemicals were of analytical reagent grade without further purification.

2.1.2. Material synthesis

V_2O_5/TiO_2 with solid sphere nanostructures: NH_4VO_3 (0.2 g, 1.7 mmol) was dissolved in 10 mL of hot deionized water with vigorous stirring. Subsequently, the dissolved NH_4VO_3 solution was dripping into 40 mL of deionized water contained with 2 mL of titanium (IV) oxysulfate solution. And then, 15 mL of glycerol were added into the mixture solution. After stirring for 30 min, the resulting reaction mixture was transferred into a 100 mL Teflon-lined autoclave and maintained at 120 °C for 48 h. After being cooled to room temperature, the sample was washed with deionized water and ethanol several times. After dried at 80 °C, the product was calcined at 550 °C for 3 h to remove the adsorbed organics. The as-prepared V_2O_5/TiO_2 composite synthesized by hydrothermal process was denoted as TV-H.

V_2O_5/TiO_2 with core–shell spherical nanostructures: The synthetic route was similar with hydrothermal route except that the absolute ethyl alcohol was taken as solvent in solvothermal process instead of deionized water. The as-prepared V_2O_5/TiO_2 composite synthesized by solvothermal process was denoted as TV-S.

Pristine TiO_2: The sample was synthesis by solvothermal process without adding NH_4VO_3.

2.2. Material characterization

The as-prepared samples were characterized by powder X-ray diffraction (XRD) on a Bruker D8 Advance X-ray diffractometer at 40,000 V and 0.04 A with Ni-filtered Cu kα radiation. Data were recorded at a scan step width of 0.02° in the range of 20–80°. The morphology of the sample was investigated by a field-emission scanning electron microscope (FEI Nova NanoSEM-230). The transmission electron microscope (TEM) and high solution TEM (HRTEM) were measured by a JEOL model JEM 2010EX instrument at an accelerating voltage of 200 kV. The specific surface area of the samples were measured by N_2 sorption at 77 K on an ASAP 2020 instrument and calculated by Brunauer–Emmett–Teller (BET) method. The optical absorption properties of the samples were analyzed using the ultraviolet-visible diffuse reflectance spectroscopy (UV–vis DRS) with an ultraviolet-visible spectrophotometer (Cary 500 Scan spectrophotometer, Varian). $BaSO_4$ was used as a reflectance standard in the UV–vis DRS experiment. The BAS Epsilon workstation was utlized to monitor the photocurrents of samples. A Bruker model A300 spectrometer was used to investigate the electron spin resonance (ESR) signals of samples. The settings of ESR were as follows: microwave power, 6.35 mW; frequency, 9.86 GHz; center field, 3512.48 G. Measurements of Raman spectra were performed on invia-Reflex Micro-Raman Spectroscopy system (Renishaw Co.) with 532 nm line of an Ar ion laser at room temperature. A 50 × microscope objective lens was used for focusing the laser beam and collection of the scattered light. The spot diameter of the focused laser beam on the sample was about 1 μm and typical spectrum acquisition time was 30 s.

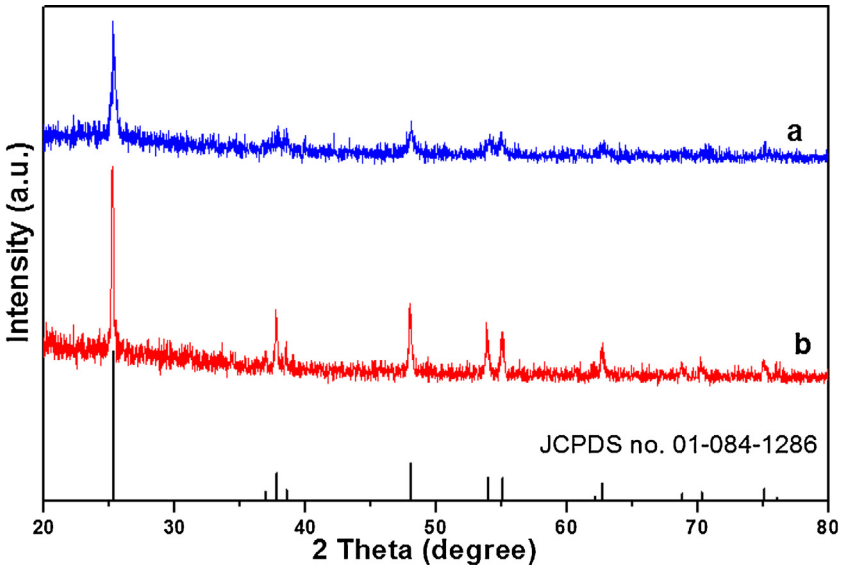

Fig. 1. Typical XRD patterns of (a) TV-H and (b) TV-S.

2.3 Photocatalytic oxidation of As(III) or As(III) removal experiments

The stock As(III) solution with a concentration of 1000 mg/L was purchased from National Analysis Center for Iron and Steel (NACIS, Beijing, China). For the experiment, the standard stock solution was diluted to 2 mg/L and adjusted to pH 4 with HCl or NaOH solution. In a typical As(III) removal experiment, 0.08 g of V_2O_5/TiO_2 was suspended in a 100 mL Pyrex glass vessel which contained 80 mL arsenic solution. The light source was 300 W Xe lamp with a 420 nm cut-off filter. During the experiment, the arsenic solution was stirred magnetically to ensure a good contact of photocatalyst with arsenic species. At given time intervals, 1 mL of the suspensions was sampled and centrifuged to remove photocatalyst. Atomic fluorescence spectrometry (PF6, Beijing purkinje general instrument Co., Ltd.) was used to analyze the As(III) content in the reaction solution.

3. Results and discussion

The XRD patterns of the as-prepared products through the hydrothermal and solvothermal process are shown in Fig. 1. As we can see, all the diffraction peaks of two samples could be readily indexed to the tetragonal phase of TiO_2 (JCPDS No. 01-084-1286). No diffraction peaks of V_2O_5 phase is observed in the patterns of either solvothermal sample (TV-S) or hydrothermal sample (TV-H). This may attribute to relatively low content and highly dispersed state of V_2O_5 in the composites [29], which is favorable for photocatalytic performance of catalysts.

Considering that the vanadium species in the as-prepared composites are still ambiguous, especially the hydrothermal sample, for the solid sphere in micrometer level is not convenient to get HRTEM characterization. Since that Raman is powerful in the identification of the structure that cannot be discerned by diffraction studies, it is adopted to identify the surface state of TiO_2 and V_2O_5 in the composites. From Fig. 2, the Raman spectrum of pure TiO_2

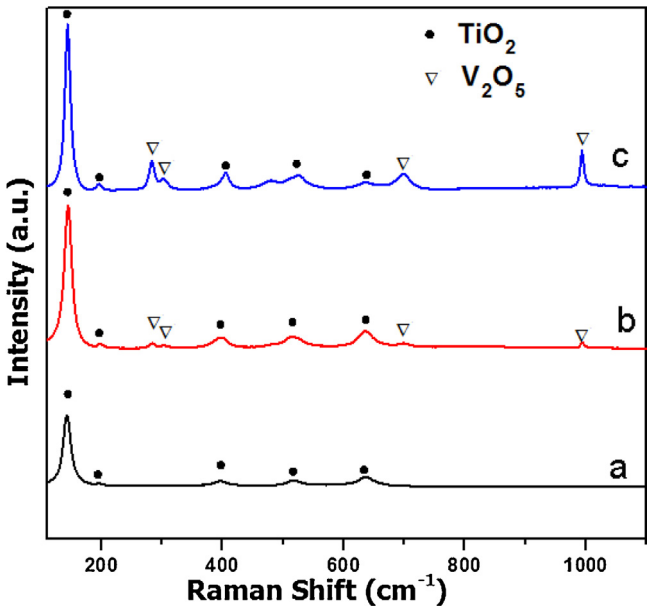

Fig. 2. Raman spectra of (a) pure TiO_2, (b) TV-H and (c) TV-S using a laser excitation line of 532 nm.

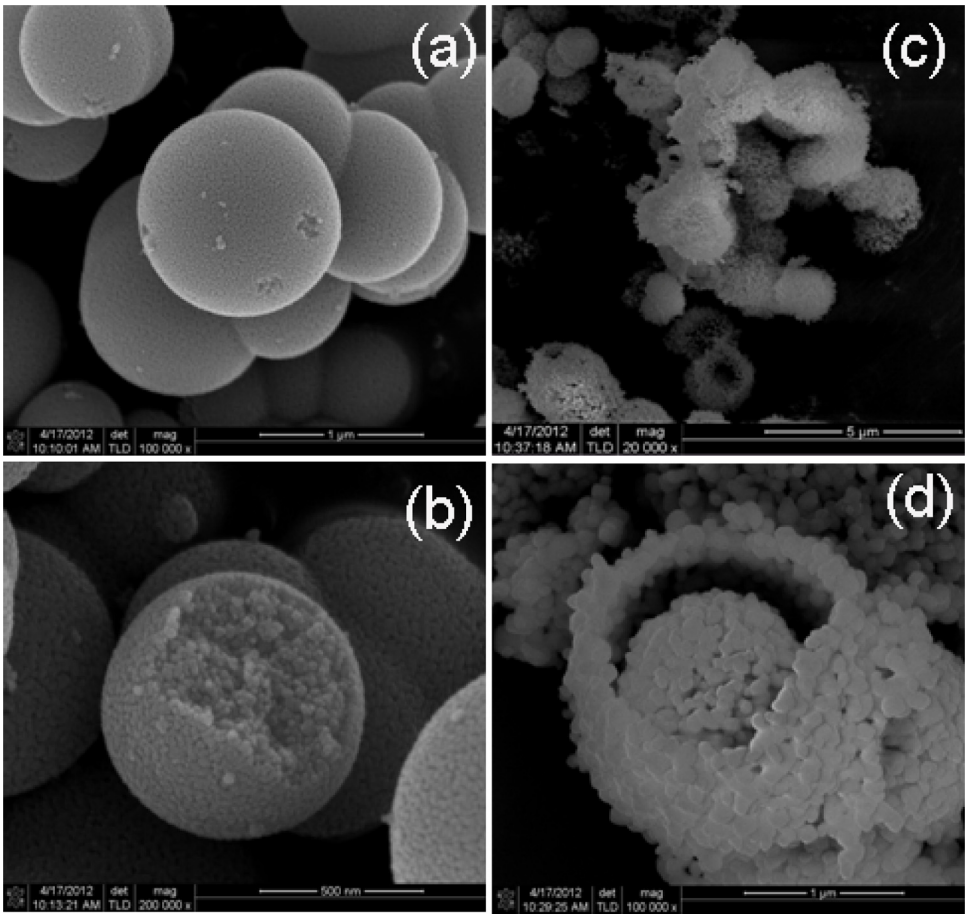

Fig. 3. Typical SEM images of TV-H (a, b) and TV-S (c, d).

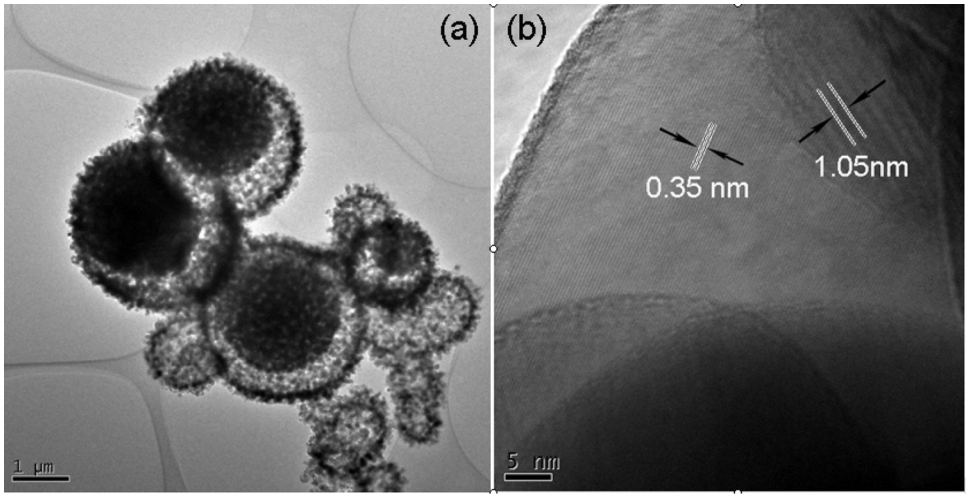

Fig. 4. TEM images (a) and HRTEM (b) images of TV-S.

shows symmetric mode of vibration of tetragonal TiO_2 identified at 396 (B_{1g}), 195 (E_g), 514 (A_{1g}), 519 (B_{1g}) and 636 cm^{-1} (E_g), where the peaks of 514 (A_{1g}) and 519 (B_{1g}) are overlapped. Importantly, the strongest E_g mode at 144 cm^{-1} arising from the vibration of the anatase structure is well resolved, which indicate that an anatase phase is formed in the as-prepared crystals [30]. No peaks of other TiO_2 crystalline phase like brookite or rutile were found. For the V_2O_5/TiO_2 composites, solid sphere sample or core–shell sphere sample, the observed band positions appear at 284 cm^{-1}, 302 cm^{-1}, 701 cm^{-1} and 993 cm^{-1} belong to the Raman signature V_2O_5 crystalline [31,32]. Here we can conclude that the TiO_2 in as-prepared composites is in the form of anatase phase while the vanadium is in the form of V_2O_5 crystalline.

The scanning electron microscopy (SEM) image reveals that the as-prepared V_2O_5/TiO_2 obtained via hydrothermal method are composed of uniform and solid spherical particles with *ca.* 1–2 μm diameters (Fig. 3a) and the solid spheres are made up of small particles with *ca.* 50 nm in dimension (Fig. 3b). Interestingly, the unique sphere-in-sphere structure with outside-sphere diameter of *ca.* 1.5 μm was observed in solvothermal sample (Fig. 3c and d). Moreover, both the yolk and the outer sphere are constituted of anomalistic grains which are irregular in shape and size. To further obtain information about the structure of solvothermal sample, the core–shell microsphere sample is characterized by TEM and HRTEM as well. In agreement with the SEM image, the TEM image of solvothermal sample (Fig. 4a) shows that the hollow sphere has a dimension of about 1–2 μm and the average dimension of the cavity is estimated to be about 500 nm. The HRTEM image of this composite shows two types of intimately contacted lattice fringes, confirming formation of the junction between TiO_2 and V_2O_5 (Fig. 4b). The lattice spacing of 0.35 nm corresponds to the interplanar distance between adjacent (1 0 1) crystallographic planes of TiO_2, while the fringe of d = 1.05 nm matches that of the (0 0 1) plane of V_2O_5 (JCPDS No. 052-0794). According to the EDS analysis (see ESI, Fig. S1), the composite was composed of O, Ti and V elements. The results suggest the ratio of TiO_2 and V_2O_5 is about 15:1 in the final products. The real content of V_2O_5 is much lower than the theoretical design value. The losing of V species may be attributed to repeated processes of washing and centrifuging after solvothermal reaction. Meanwhile this result is in accordance with XRD pattern of composites, in which no peak of V_2O_5 was found.

To get more information about spatial distribution of titanium and vanadium in the multi-level structures, the elemental composition was also confirmed from mapping analysis of a single core–shell sphere. As the result shown in Fig. 5, the TiO_2 and V_2O_5 were well-distributed in the core as well as on the shell.

The N_2 adsorption–desorption isotherm and the pore size distribution curve (Fig. 6) demonstrated that both the TV-S and the TV-H samples were presented as mesoporous structure with narrow pore size distribution centered at about 14–17 nm. The BET surface area (S_{BET}) and the pore volume (V_p) of TV-S sample were determined as 79 m^2/g and 0.37 cm^3/g, which are larger than that of TV-H sample (S_{BET} = 40 m^2/g and V_p = 0.14 cm^3/g).

On the basis of structural characterization results described above, it is instructive to compare the photocatalytic performance of the samples under visible light irradiation. Thus these two as-prepared V_2O_5/TiO_2 composites were utilized as photocatalysts in the removal of As(III) in aqueous solution under visible light irradiation. It has already been reported that the As(III) species is very stable under visible light illumination [33]. Under dark condition, the absorption behavior of arsenic (III) over solid sphere and core–shell sphere sample are displayed in the imaginary lines in Fig. 7a and b, respectively. By comparison, the absorption of As(III) over core–shell sphere sample is stronger than that over solid sphere sample, which is owing to the relative larger specific surface area of core–shell sphere sample. It is well known that the absorption of substrate on catalysts is closed-related to the subsequent heterogeneous photocatalytic reaction. Therefore, the arsenic species absorbed on samples is benefit for the photo oxidation reaction from As(III) to As(V). With the presence of core–shell sphere sample, the concentration of As(III) in aqueous decline rapidly and the removal ratio of As(III) is up to 93% after 80 min of visible illumination (Fig. 7a). While in the solid sphere photocatalytic system, there are still 37% of As(III) remain in aqueous solution after the same time illumination (Fig. 7b). It can be concluded that the photocatalytic performance for As(III) oxidation over core–shell sphere sample is superior to that over solid sphere sample.

Seeking the reasons of different performance over TV-S sample and TV-H sample will be constructive to study the relationship between structure, composition and performance of this kind of photocatalysts. Thus it is imperative to find out reasons for superior ability of photocatalytic oxidation over core–shell sphere sample.

As now well known that specific surface area always has a big impact on the optical property of photocatalyst, for higher specific surface area could absorb more target pollutant and offer more reactive active sites for photocatalysis [34]. So the specific surface area becomes higher priority influencing factor being considered.

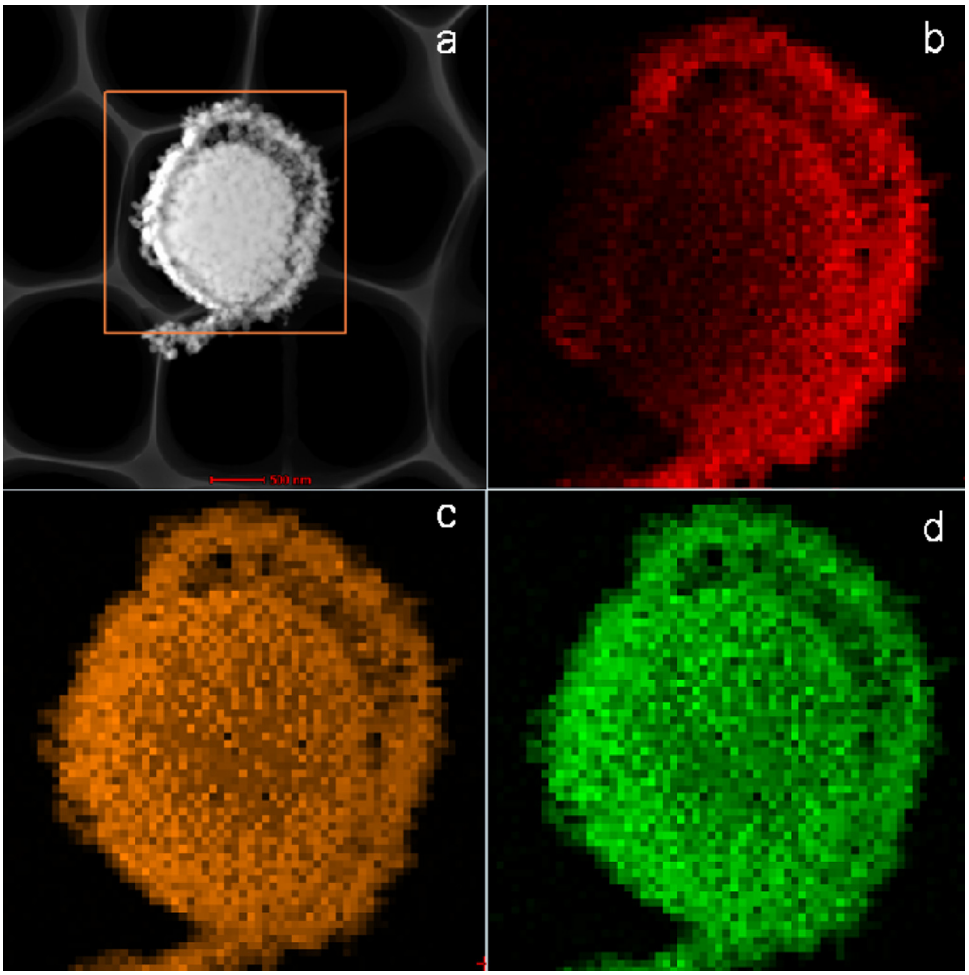

Fig. 5. Energy dispersive X-ray (EDX) elemental mapping analysis of TV-S sample; (b–d) atomic mapping of O, Ti and V, respectively.

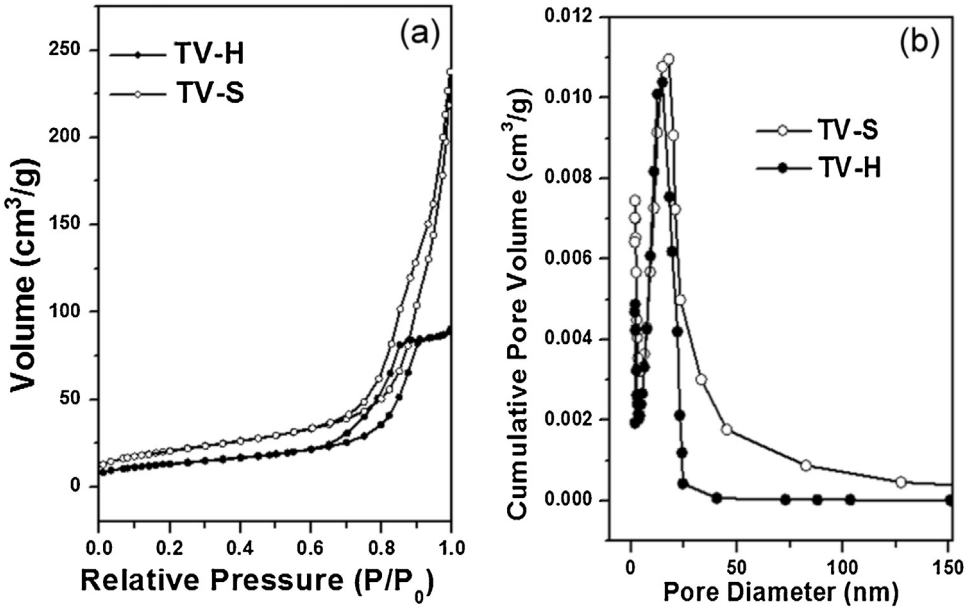

Fig. 6. N_2 sorption isotherms (a) and corresponding pore size distribution curves (b) of TV-H and TV-S.

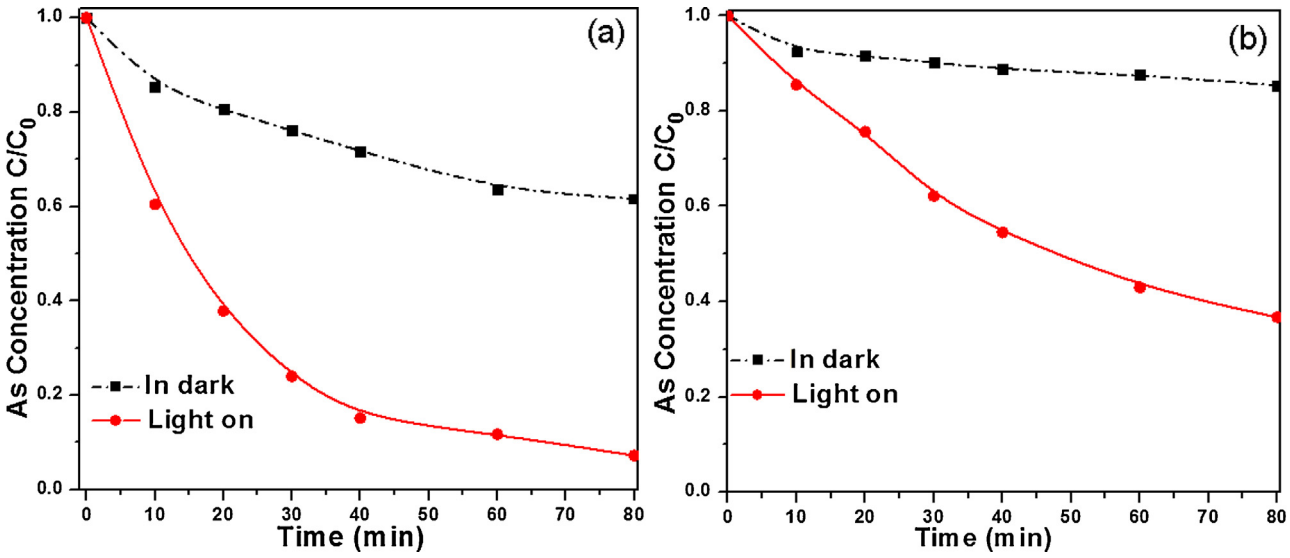

Fig. 7. Temporal changes in the concentration of As(III) in the dark and under visible light: (a) Solvothermal sample with core–shell structure; (b) Hydrothermal sample with solid sphere structure.

As mentioned above, the BET specific surface area of core–shell sphere sample is 79 m^2/g and that of solid sphere sample is 40 m^2/g. Combining the absorption capacities of these two samples in the dark, it comes to a conclusion that higher specific surface area plays a certain promotion role in adsorption of As(III) and subsequent photocatalytic oxidation processes of As(III).

It has been well known that the microstructures always impact the optical property of photocatalysts [35]. The optical properties of the products were measured by UV–vis DRS and the corresponding absorption spectrum is shown in Fig. 8a. The absorption edges of Pristine TiO_2 samples appeared at 382 nm. In the presence of V_2O_5, both two samples exhibit absorption in the visible light range, and their absorption edges were clearly shifted to 450–500 nm, which suggest these two samples are capable of responding to visible light. Moreover the core–shell structure sample exhibits stronger light absorption than solid sphere sample, which may owe to the distinguishing microstructure between these two samples. Due to the unique core–shell microstructure, once the light is transmitted into the shell, it would reflect on the inner surface of shell for multiple times and trapped in the shell [36]. This phenomenon would greatly improve the light harvest ability, as shown in Fig. 8b.

To further confirm that the core–shell sphere sample have stronger capacity in visible light absorption, the transient photocurrents are carried out to distinguish the charges of photoelectrochemical responses and verify the formation and transfer of electrons in materials.

As shown in Fig. 9, core–shell sphere sample and solid sphere sample exhibit different visible light photocurrent. The generation of photocurrent is attributed to the excited electrons from surface of materials to ITO glass. And it is obvious that the core–shell sphere sample shows a stronger visible light photocurrent response than that of solid sphere sample, which is in good accordance with photocatalytic oxidation of As(III) under visible light. This photocurrent enhancement of core–shell sphere sample may be attributed to more separated electrons and holes migrating on the surface. When the incident light is cut off, the photocurrent of two samples descend slowly to initial point, which means that the photo-induced carrier lifetime of two samples was almost the same. This photocurrent experiment verifies that the core–shell structure can facilitate the migration of photo-induced carrier over surface of material.

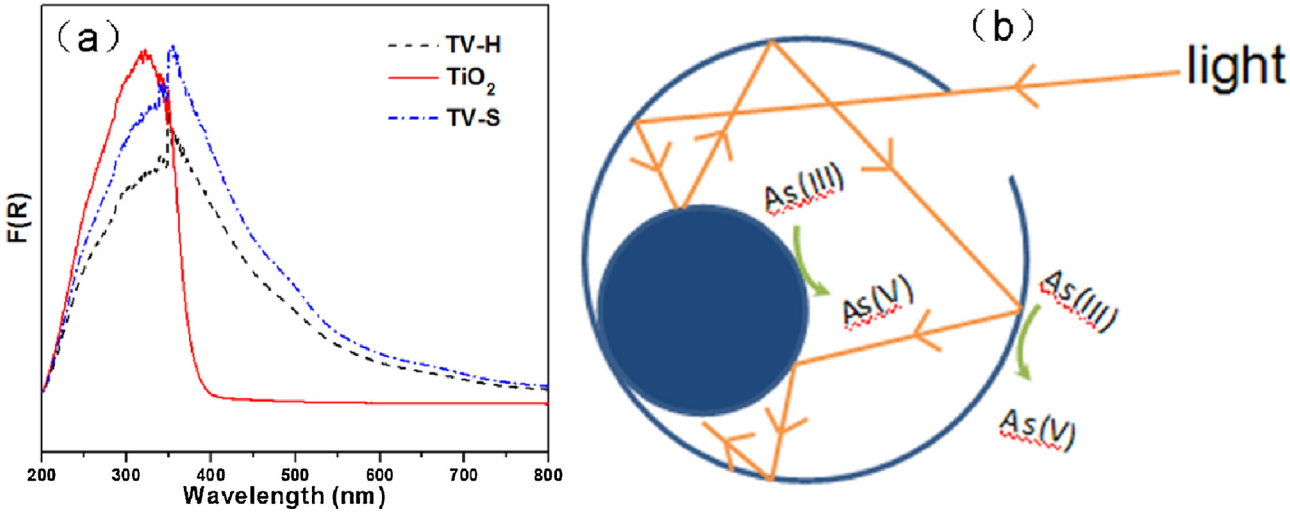

Fig. 8. (a)UV-DRS spectra of pure TiO_2, TV-H and TV-S; (b) the schematic diagram of substrate and light absorption in core–shell sphere nanocomposites.

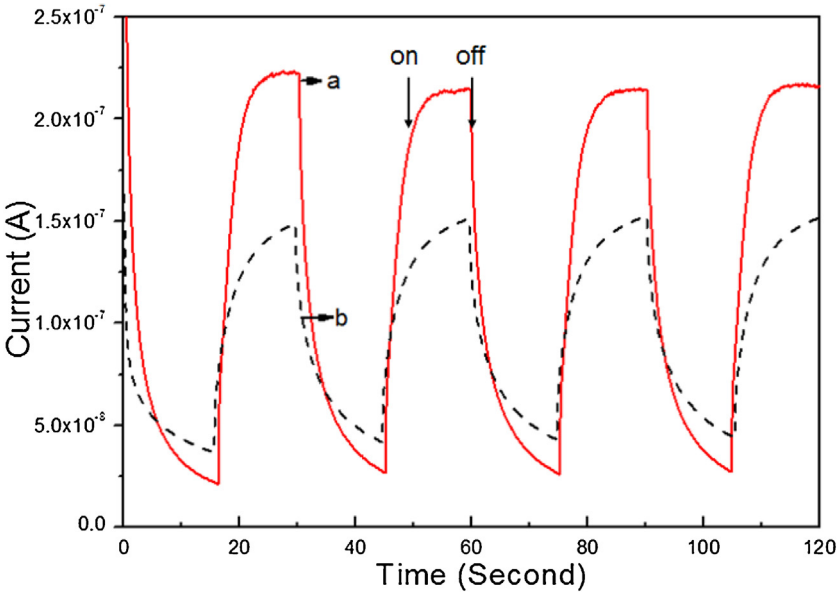

Fig. 9. The photocurrent generated by TV-S (a) and TV-H (b) under visible light irradiation.

It is well known that the process of photocatalytic oxidation for As(III) involves diverse active species, such as photo-generated holes, •OH and $O_2^{\bullet-}$. Even in photocatalytic oxidation of As(III) in TiO_2 system under UV light, there is still no consensus on the mechanism about the mainly functional active species [37–40]. Therefore, it is of great significance to identify the main active species in the process of photocatalytic oxidation reaction for As(III) under visible light. In order to identify the reactive species responsible for As(III) photooxidation over V_2O_5/TiO_2 composites, ESR measurement is carried out with core–shell sample illuminated under visible light. Once the •OH and O_2^- were generated by irradiation, they would be trapped by DMPO and the spin-adducts (DMPO-•OH and DMPO- O_2^-) can be detected by ESR instrument. As shown in Fig. 10a and b, after minutes of visible light irradiation, six characteristic peaks of DMPO-$O_2^{\bullet-}$ adduct was observed in the methanol solvent, while in the dark no obvious peaks was observed. However, whether in darkness or under visible light irradiation, there are no ESR signals for the spin adducts DMPO-•OH, which suggests that there is no •OH produced in the V_2O_5/TiO_2-DMPO-H_2O system. Therefore, the O_2^- is generated and acts as an effective oxidant in the core-shell V_2O_5/TiO_2 photocatalytic system under visible light.

Furthermore, the photo-generated hole (h^+) is usually considered as an important active species during photocatalytic process. Hence, it is necessary to determinate whether photo-generated holes participate in photooxidation reaction. In this experiment, ammonium oxalate is used as a hole-scavenger to estimate the influence of holes on the photooxidation of As(III) over V_2O_5/TiO_2 with core–shell microstructure. As shown in Fig. 10c, it is interesting to discover that the photo-oxidation process of As(III) is

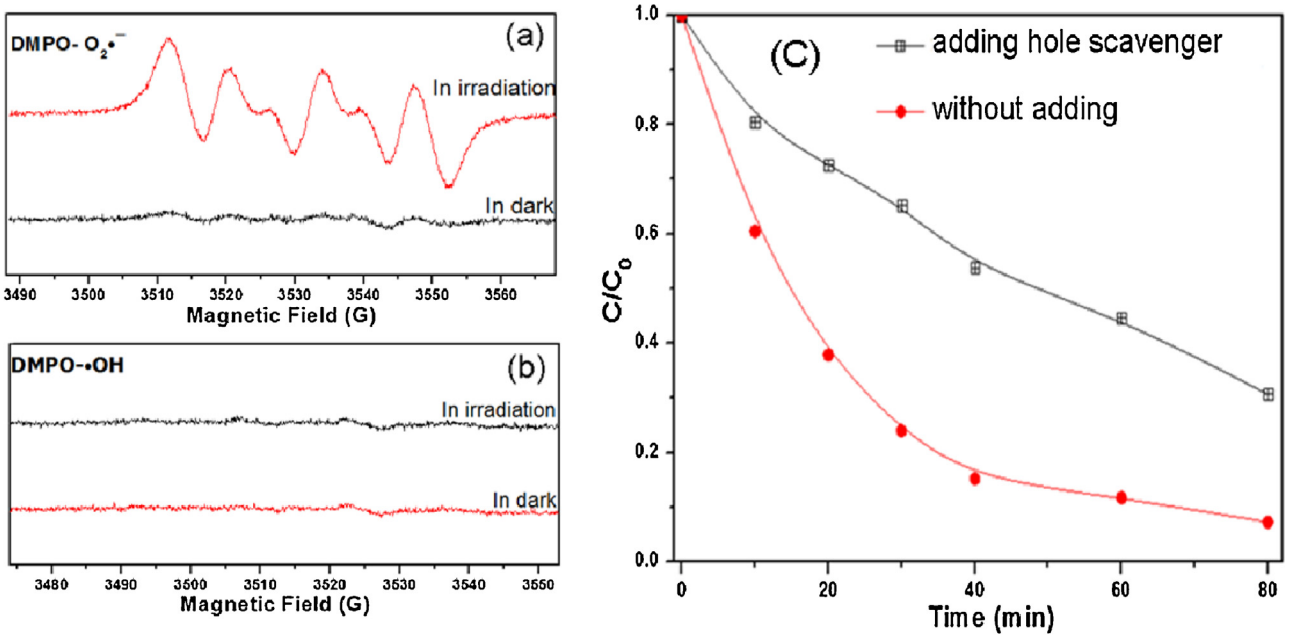

Fig. 10. (a) DMPO-$O_2^{\bullet-}$ adducts are detected for TV-S sample in methanol; (b) DMPO-•OH adducts are detected for TV-S sample in water; (c) The role of ammonium oxalate in Photo-oxidation of As(III) over TV-S under visible light irradiation.

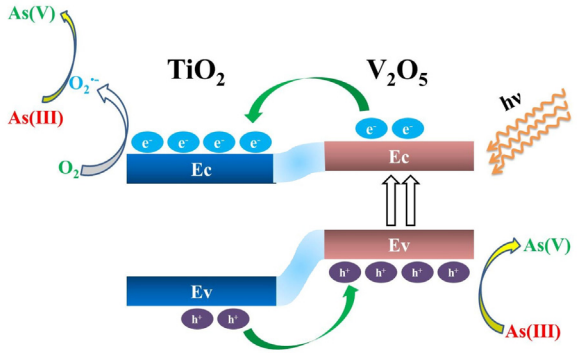

Fig. 11. Proposed mechanisms for the photo-oxidation of As(III) over V_2O_5/TiO_2 composite under the visible light Ev = valence band, Ec = conduction band, h^+ = hole, e^- = electron.

remarkable inhibited by adding ammonium oxalate, indicating that the photo-generated hole is also an effective active species in this system. So, to summarize, h^+ and $O_2^{\bullet-}$ are recognized as the mainly active species of the oxidation of As(III) over V_2O_5/TiO_2 composite.

On the basis of experimental results above and early reports [24,31], a possible photocatalysis process for the oxidation of As(III) in the visible light irradiated V_2O_5/TiO_2 system was conclude and shown in Fig. 11. Under the visible light illumination, the surface complex can be excited to generate electrons and holes via V_2O_5, and the electrons in the conduction band of V_2O_5 are meteorically shifted to the conduction band of TiO_2. The oxygen absorbed on the surface of composite will be reduced into superoxide radicals. Meanwhile, the corresponding produced holes in the valence band of TiO_2 would migrate to the valence band of V_2O_5. Therefore the As(III) will be oxidized directly by the generated holes as well as the superoxide radicals in the system.

4. Conclusions

In summary, the V_2O_5/TiO_2 composites with core–shell sphere structure and solid sphere structure are synthesized by solvothermal and hydrothermal method, respectively. The core–shell sphere sample exhibit superior performance for As(III) oxidation, which may be attributed to three reasons. First, the specific surface area of core–shell sample is much higher, which provides larger effective area and more active sites for absorption, leading to more efficient subsequent photocatalytic process. Second, the particular core in shell structure is believed to facilitate the multiple reflections of light and transportation of substrate molecules between the cavities. Third, the core–shell sample is in favor of the faster moving of photogenerated carriers to surface in the role of internal electrical field, which accordingly promote the separation of photogenerated holes and electrons. In the V_2O_5/TiO_2 photocatalysis system As(III) is oxidized by the cooperative effect of superoxide radical and photo-generated holes. These findings could deepen the comprehending of multi-level-structure materials' particular properties and offer an appropriate strategy for the feasible treatment of As(III) in water.

Acknowledgements

The work is supported by National Natural Science Foundation of China (21473031, 21303244, 21203026), National Basic Research Program of China (973 Program: 2013CB632405), Natural Science Foundation of Fujian province (2015J01057), Scientific Project of Putian Science and Technology Bureau (2013S03(3)).

Appendix A. Supplementary data

Supplementary data associated with this article can be found, in the online version, at http://dx.doi.org/10.1016/j.apcatb.2015.11.014.

References

[1] Y. Xia, J. Liu, Toxicol. 198 (2004) 25–29.
[2] K.C. Saha, Crit. Rev. Environ. Sci. Technol. 33 (2003) 127–163.
[3] A.A. Meharg, A. Raab, Environ. Sci. Technol. 44 (2010) 4395–4399.
[4] M. Bissen, M.-M. Vieillard-Baron, A.J. Schindelin, F.H. Frimmel, Chemosphere 44 (2001) 751–757.
[5] X. Zhao, B. Zhang, H. Liu, J. Qu, J. Hazard. Mater. 184 (2010) 472–476.
[6] G. Caumette, I. Koch, E. Estrada, K.J. Reimer, Environ. Sci. Technol. (2011) 9917–9923.
[7] X. Guan, J. Du, X. Meng, Y. Sun, B. Sun, Q. Hu, J. Hazard. Mater. 215–216 (2012) 1–16.
[8] M.I. Litter, M.E. Morgada, J. Bundschuh, Environ. Pollut. 158 (2010) 1105–1118.
[9] M.T. Emett, G.H. Khoe, Water Res. 35 (2001) 649–656.
[10] W. Driehaus, R. Seith, M. Jekel, Water Res. 29 (1995) 297–305.
[11] M.-J. Kim, J. Nriagu, Sci. Total Environ. 247 (2000) 71–79.
[12] M. Pettine, L. Campanella, F.J. Millero, Geochim. Cosmochim. Acta 63 (1999) 2727–2735.
[13] H. Yang, W.Y. Lin, K. Rajeshwar, J. Photochem. Photobio. A: Chem. 123 (1999) 137–143.
[14] M.A. Ferguson, M.R. Hoffmann, J.G. Hering, Environ. Sci. Technol. 39 (2005) 1880–1886.
[15] J. Ryu, W. Choi, Environ. Sci. Technol. 38 (2004) 2928–2933.
[16] P. Mondal, C.B. Majumder, B. Mohanty, J. Hazard. Mater. 137 (2006) 464–479.
[17] I.A. Katsoyiannis, T. Ruettimann, S.J. Hug, Environ. Sci. Technol. 42 (2008) 7424–7430.
[18] S. Bordoloi, S.K. Nath, S. Gogoi, R.K. Dutta, J. Hazard. Mater. 260 (2013) 618–626.
[19] Y. Bessekhouad, D. Robert, J.V. Weber, Catal. Today. 101 (2005) 315–321.
[20] Y. Bessekhouad, D. Robert, J.V. Weber, J. Photochem. Photobio. A: Chem. 163 (2004) 569–580.
[21] E.V. Skorb, E.A. Ustinovich, A.I. Kulak, D.V. Sviridov, J. Photochem. Photobio. A: Chem. 193 (2008) 97–102.
[22] T. Ohno, F. Tanigawa, K. Fujihara, S. Izumi, M. Matsumura, J. Photochem. Photobio. A: Chem. 118 (1998) 41–44.
[23] G. Xiao, X. Wang, D. Li, X. Fu, J. Photochem. Photobio. A: Chem. 193 (2008) 213–221.
[24] J. Liu, R. Yang, S. Li, Rare Metals 25 (2006) 636–642.
[25] M. Bayati, F. Golestani-Fard, A. Moshfegh, Catal. Lett. 134 (2010) 162–168.
[26] B. Wen, C. Liu, Y. Liu, New J. Chem. 29 (2005) 969–971.
[27] C. Wang, Z. Deng, Y. Li, Inorg. Chem. 40 (2001) 5210–5214.
[28] H. Li, Z. Bian, J. Zhu, Y. Huo, H. Li, Y. Lu, J. Am. Chem. Soc. 129 (2007) 4538–4539.
[29] J. Liu, R. Yang, S. Li, J. Rare Earth 25 (2007) 173–178.
[30] W. Zhang, Y. He, M. Zhang, Z. Yin, Q. Chen, J. Phys. D: Appl. Phys. 33 (2000) 912–916.
[31] Y. Wang, Y. Su, L. Qiao, L. Liu, Q. Su, C. Zhu, X. Liu, Nanotechnology 22 (2011) 225702.
[32] B.M. Reddy, A. Khan, Y. Yamada, T. Kobayashi, S. Loridant, J. Volta, J. Phys. Chem. B 107 (2003) 5162–5167.
[33] Q. Tian, J. Zhuang, J. Wang, L. Xie, P. Liu, Appl. Catal. A: Gen. 425–426 (2012) 74–78.
[34] A. Fujishima, K. Honda, Nature 238 (1972) 37.
[35] J. Hu, S. Weng, Z. Zheng, Z. Pei, M. Huang, P. Liu, J. Hazard. Mater. 264 (2014) 293–302.
[36] H. Li, Z. Bian, J. Zhu, D. Zhang, G. Li, Y. Huo, H. Li, Y. Lu, J. Am. Chem. Soc. 129 (2007) 8406–8407.
[37] W. Leng, H. Fei, J. Zhang, Environ. Sci. Technol. 45 (2011) 9818–9819.
[38] H. Fei, W. Leng, X. Li, X. Cheng, Y. Xu, J. Zhang, C. Cao, Environ. Sci. Technol. 45 (2011) 4532–4539.
[39] H. Lee, W. Choi, Environ. Sci. Technol. 36 (2002) 3872–3878.
[40] W. Choi, J. Yeo, J. Ryu, T. Tachikawa, T. Majima, Environ. Sci. Technol. 44 (2010) 9099.